

# COSMIC RAY ACCELERATION AT RELATIVISTIC SHOCK WAVES WITH A ‘REALISTIC’ MAGNETIC FIELD STRUCTURE

Jacek Niemiec

*Instytut Fizyki Jądrowej Polskiej Akademii Nauk,  
ul. Radzikowskiego 152, 31-342 Kraków, Poland*

*Jacek.Niemiec@ifj.edu.pl*

and

Michał Ostrowski

*Obserwatorium Astronomiczne, Uniwersytet Jagielloński,  
ul. Orla 171, 30-244 Kraków, Poland*

## ABSTRACT

The process of cosmic ray first-order Fermi acceleration at relativistic shock waves is studied with the method of Monte Carlo simulations. The simulations are based on numerical integration of particle equations of motion in a turbulent magnetic field near the shock. In comparison to earlier studies, a few ‘realistic’ features of the magnetic field structure are included. The upstream field consists of a mean field component inclined at some angle to the shock normal and finite-amplitude sinusoidal perturbations imposed upon it. The perturbations are assumed to be static in the local plasma rest frame. Their flat or Kolmogorov spectra are constructed with randomly drawn wave vectors from the wide range ( $k_{min}, k_{max}$ ). The downstream field structure is derived from the upstream one as compressed at the shock. We present and discuss particle spectra and angular distributions obtained at mildly relativistic sub- and superluminal shocks. We show that particle spectra diverge from a simple power-law, the exact shape of the spectrum depends on both the amplitude of the magnetic field perturbations and the wave power spectrum considered. Features such as spectrum hardening before the cut-off at oblique subluminal shocks and formation of power-law tails at superluminal ones are presented and discussed. The simulations have been also performed for parallel shock waves. The presence of finite-amplitude magnetic field perturbations leads to the formation of locally oblique field configurations at the shock and the respective magnetic field compressions. This

results in the modification of the particle acceleration process, introducing some features present in oblique shocks, e.g., particle reflections from the shock. For the first time, we demonstrate for parallel shocks a (non-monotonic) variation of the accelerated particle spectral index with the turbulence amplitude. At the end, a few astrophysical consequences of the results we obtained are mentioned.

*Subject headings:* acceleration of particles, cosmic rays, gamma rays:bursts, methods: numerical, relativity, shock waves

## 1. INTRODUCTION

Relativistic shock waves are postulated to be responsible for a number of phenomena of high-energy astrophysics. Many sources of high-energy radiation appear at the same time to involve highly relativistic plasma flows, indicating the relativistic shocks being the acceleration sites of energetic particles producing high-energy emission. The observed examples of such flows/shocks can be hot spots in radio galaxies, parsec-scale jets in blazars, jets in galactic ‘microquasars’, gamma ray burst sources, and pulsar winds. Understanding of particle acceleration processes at relativistic shocks is essential in a study of these objects.

At relativistic shock waves the bulk flow velocity is comparable to particle velocity. This leads to anisotropy of particle angular distribution, which can substantially influence the process of particle acceleration. The first consistent method to tackle the problem for a parallel shock wave, where the mean magnetic field is parallel to the shock velocity, was proposed by Kirk & Schneider (1987a). Generalizing the diffusive approach by explicit treatment of the particle distribution function anisotropy, they constructed stationary solutions of the pitch-angle diffusion equation on both sides of the shock. The requirement of distribution function continuity at the shock allowed them to match the upstream and downstream solutions by taking into account a sufficient number of high-order terms in particle anisotropy. The solution was obtained from numerical fitting of the respective coefficients. This semi-analytic procedure yielded the power-law index of the resulting spectrum, as well as the anisotropic particle angular distribution at the shock. The spectral indices for the phase space distribution function derived with this method for relativistic shocks — with the compression ratio  $R = 4$  — were only slightly different from the  $\alpha = 4$  value obtained in the nonrelativistic case. These findings were later confirmed by Kirk & Schneider (1987b) by the method of particle Monte Carlo simulations (see also Ellison, Jones, & Reynolds 1990).

An extension of the above approach was proposed by Heavens & Drury (1988), who modified the method to treat more general conditions at the shock. They investigated the

fluid dynamics of relativistic shock waves and applied the results to calculate spectral indices of particles accelerated at such shocks. For a parallel shock wave propagating into cold electron-proton or electron-positron plasma, they found that the particle spectral index depends on the form of the wave power spectrum, in contrast to the nonrelativistic case. The spectral indices obtained were close to the respective values given by the nonrelativistic formula,  $\alpha = 3R/(R - 1)$ . Kirk & Heavens (1989) considered the acceleration processes in shocks with magnetic fields oblique to the shock normal. For the subluminal shock configurations studied they assumed magnetic moment conservation for particles interacting with the shock. This assumption restricted the validity of their considerations to the case of a weakly perturbed magnetic field. The important result of this work was that oblique shocks lead to flatter spectra than parallel ones, a spectrum could be even as flat as  $\alpha \approx 3$  in cases where the shock velocity along magnetic field lines is close to the speed of light. This feature arises due to effective multiple reflections of anisotropically distributed upstream particles from the compressed downstream magnetic field. However, as pointed out by Begelman & Kirk (1990), most field configurations in relativistic shocks lead to superluminal conditions for the acceleration process. Therefore, unless there is strong particle scattering across field lines, particles are not able to cross the shock front repeatedly, and diffusive acceleration is inefficient. Instead, particle energy gains are due to the shock-drift acceleration process, which involves a single shock transmission of upstream particles downstream of the shock (Webb, Axford, & Terasawa 1983; Drury 1983).

The above approximations rely on an assumption of a weakly perturbed magnetic field, where cross-field diffusion does not play a significant role. However, in astrophysical shocks one may expect large amplitude MHD waves to occur. In such conditions, scattering of particles is not exclusively related to resonant interactions with the magnetic field fluctuations, as in the small amplitude wave limit. In this case, neither does the Fokker-Planck equation properly describe the particle transport nor does the particle magnetic moment conservation hold for oblique shocks (Decker & Vlahos 1985; Ostrowski 1991). Then, the particle acceleration process has to be investigated with the help of numerical methods.

A role of finite-amplitude magnetic field perturbations in forming a particle spectrum was investigated by a number of authors using the Monte Carlo particle simulations (e.g., Ellison et al. 1990; Ostrowski 1991, 1993; Ballard & Heavens 1992; Naito & Takahara 1995; Bednarz & Ostrowski 1996, 1998). The main result of these considerations was the finding of a direct dependence of the derived particle spectra on the conditions near the shock. The power-law spectra can be either very steep or very flat for different mean magnetic field inclinations to the shock normal and different amplitudes of perturbations, where changes of the particle spectral index can be non-monotonic with an increasing field perturbations amplitude (Ostrowski 1991, 1993).

The process of the first-order Fermi acceleration at ultrarelativistic shocks ( $\gamma \gg 1$ ) has been studied in the last few years by a number of authors (Bednarz & Ostrowski 1998; Gallant & Achterberg 1999; Gallant et al. 1999; Achterberg et al. 2001; Kirk et al. 2000; Lemoine & Pelletier 2003). All these approaches yield consistent estimates of the asymptotic ( $\gamma \rightarrow \infty$ ) spectral index  $\alpha \approx 4.2 \div 4.3$  in the limit of highly turbulent conditions near the shock (cf. Ostrowski & Bednarz 2002). In conditions with medium amplitude magnetic field perturbations, the particle spectra generated at ultrarelativistic shocks can be much steeper than those obtained in the asymptotic limit, as seen in the simulations of Bednarz & Ostrowski (1998).

Numerical investigations of the first-order Fermi process are based on simulations of particle motion in a turbulent magnetic field near the shock front. One possible method is to use the pitch-angle diffusion model to study particle transport in a way similar to the quasi-linear analytic approximation. Such an approach was first presented by Kirk & Schneider (1987b), and essentially the same technique was independently elaborated for oblique shocks by Ostrowski (1991) (see also Bednarz & Ostrowski 1996, 1998). In this approach, a particle is assumed to move in a regular magnetic field along its undisturbed ‘adiabatic’ trajectory and the influence of the turbulent field on the orbit is described by discrete, uncorrelated, small amplitude particle pitch-angle perturbations in finite time intervals. Depending on the model parameters — the mean time between successive scattering acts and the scattering amplitude — one is able to simulate situations with different magnetic field configurations and different turbulence amplitudes.

The other and perhaps more basic method of numerical simulations is to specify the entire magnetic field in the space near the shock and to integrate particle equations of motion in such a ‘realistic’ field. However, this method is much more difficult to implement because precise numerical calculations of particle trajectories in a wide wave vector range spectrum require usually excessive simulation times. Due to this fact, the two early papers adopting this technique for relativistic shock waves had to apply very simple models of a turbulent magnetic field. Ballard & Heavens (1992) considered a highly disordered magnetic field with vanishing regular component, equivalent to discussing a parallel highly turbulent shock. The field was described in the Fourier space by the Kolmogorov power-law spectrum in the very limited wave vector range,  $k_{max}/k_{min} \approx 20$ . In their approach, the upstream and downstream turbulent fields were unrelated and, additionally, a new turbulent field pattern was selected at each particle shock crossing. Because of the restricted dynamical range for the magnetic field perturbations, the resulting particle spectra were formed in a limited energy range near the injection energy. A different approach was presented by Ostrowski (1993). In his work, the magnetic field consisted of the regular component and the perturbations, described as a superposition of a few sinusoidal static waves of finite amplitude, oriented randomly

with respect to the mean field. For each particle of a given energy there were three wave vector ranges, containing short, resonance, and long waves with the flat power spectrum. When in the course of the acceleration process a particle energy increased, the respective short waves were replaced by the existing previously resonance wave vectors, the resonance waves by the long ones, and a new set of waves was selected for the long waves. With this procedure, one was able to study particle acceleration to very high energies, which allowed for an accurate determination of the spectral indices in an energy range not influenced by the initial conditions. The spectra obtained by Ostrowski for parallel shocks were systematically flatter than those calculated by Ballard & Heavens (1992) (see discussion in Ostrowski 1993).

The purpose of our present work is to simulate the first-order Fermi acceleration process at (mildly) relativistic shock waves, propagating in more realistically modeled perturbed magnetic fields. This involves the use of a wide wave vector range turbulence with the power-law spectrum and continuity of the magnetic field across the shock front, according to the respective matching conditions. Particle trajectories are calculated by integrating their equations of motion in such fields. Both sub- and superluminal mean magnetic field configurations are studied, as well as the particular case of parallel shocks. Angular distributions and wide-energy particle spectra are derived in a range of model parameters. We show that the particle spectra diverge from a simple power-law in a full energy range considered, yielding in some cases interesting spectral features. A number of previously obtained results are also reproduced. The simulation method and the magnetic field structure assumed are described below, in Section 2. The results are presented in Section 3 and finally summarized and discussed in Section 4.

Below, the speed of light  $c$  is used as the velocity unit. All calculations are performed in the respective local plasma (upstream or downstream) rest frames. The upstream (downstream) quantities are labeled with the index ‘1’ (‘2’). We consider ultrarelativistic particles with  $p = E$ . In units we use in our simulations, a particle of an unit energy moving in an uniform mean upstream magnetic field  $B_{0,1}$ , has the unit maximum (for  $p_{\perp} = E$ ) gyroradius  $r_g(E = 1) = 1$  and the respective resonance wave vector  $k_{res}(E = 1) = 2\pi$ .

## 2. SIMULATIONS

In our simulations, trajectories of ultrarelativistic test particles are derived by integrating their equations of motion in a perturbed magnetic field. A relativistic shock wave is considered to be a planar discontinuity, propagating in a rarefied (collisionless) electron-proton plasma with a turbulent magnetic field frozen in it. Upstream of the shock, the field is assumed to consist of the uniform component  $\mathbf{B}_{0,1}$ , inclined at some angle  $\psi_1$  to the shock

normal, and finite-amplitude perturbations imposed upon it. The irregular component has either a flat ( $F(k) \sim k^{-1}$ ) or a Kolmogorov ( $F(k) \sim k^{-5/3}$ ) wave power spectrum in the (wide) wave vector range ( $k_{min}, k_{max}$ ). The perturbations are assumed to be static in the local plasma rest frame, both upstream and downstream of the shock. Thus, the possibility of second-order Fermi acceleration is excluded from our considerations. The shock propagates with velocity  $u_1$  with respect to the upstream plasma. The magnetic field is assumed to be dynamically unimportant and its downstream structure, together with the downstream flow velocity  $u_2$ , are obtained from hydrodynamic jump conditions for shocks propagating in the cold electron-proton plasma. Derivation of the shock compression ratio, defined in the shock rest frame as  $R = u_1/u_2$ , is based on the approximate formulae derived by Heavens & Drury (1988). For the case of the shock propagating with velocity  $u_1 = 0.5c$  studied in the paper, these formulae give  $R \simeq 5.11$ . For the shock velocity  $u_1 = 0.9c$ , the shock compression ratio is  $R \simeq 3.92$  and for  $u_1 = 0.98c$   $R \simeq 3.29$ . The acceleration process is considered in the particle energy range where radiative (and other) losses can be neglected.

## 2.1. Magnetic Field Structure

The ‘turbulent’ ( $\equiv$  perturbed) magnetic field component upstream of the shock is modeled as a superposition of sinusoidal static waves of finite amplitude (cf. Ostrowski 1993). In our simulations, in the magnetic field related primed coordinate system<sup>1</sup>, they take the form:

$$\delta B_{x'} = \sum_{l=1}^{294} \delta B_{x'l} \sin(k_{x'y'}^l y' + k_{x'z'}^l z'), \quad (1)$$

where  $k_{x'y'}^l + k_{x'z'}^l = k_{x'}^l$  (see below), and analogously for  $\delta B_{y'}$  and  $\delta B_{z'}$  components. Such a form of  $\delta \mathbf{B}$  ensures that  $\nabla \cdot \mathbf{B} = 0$ . The index ‘ $l$ ’ enumerates the wave vector range from which the wave vectors  $k_i^l$  ( $i = x', y', z'$ ) are randomly drawn. The components  $k_{x'y'}^l$ ,  $k_{x'z'}^l$  of the wave vectors  $k_{x'}^l$  are selected by choosing a random phase angle  $\phi_{x'}^l$ , so that  $k_{x'y'}^l = k_{x'}^l \cos \phi_{x'}^l$  and  $k_{x'z'}^l = k_{x'}^l \sin \phi_{x'}^l$ , and analogously for other components. The wave vectors span the range ( $k_{min}, k_{max}$ ), where  $k_{min} = 0.0001$  and  $k_{max} = 10$ . The selected form of the perturbations and the method of  $k_i^l$  vector components drawing both produce isotropic turbulence. It has been checked that the number of 294 wave vector ranges used

---

<sup>1</sup>In the upstream plasma rest frame the  $x$ -axis of the (unprimed) Cartesian coordinate system  $(x, y, z)$  is perpendicular to the shock surface. The shock wave moves in the negative  $x$  direction and the regular magnetic field lies in the  $xy$ -plane. The primed system  $(x', y', z')$  is obtained from the unprimed one by its rotation about the  $z$ -axis by an angle  $\psi_1$ , so that the  $x'$ -axis is directed along  $\mathbf{B}_{0,1}$ .

in the simulations is well sufficient for the perturbed magnetic field to diffusively scatter particles. Using larger number of waves would result in respectively longer simulation times.

The wave amplitudes  $\delta B_{il}$  are selected at random to satisfy  $\delta B_l^2 = \sum_i \delta B_{il}^2$  and the amplitudes  $\delta B_l$  are chosen to reproduce the turbulence power spectrum assumed. In the wave vector range considered, this spectrum can be written:

$$\delta B_l(k) = \delta B_l(k_{min}) \left( \frac{k}{k_{min}} \right)^{(1-q)/2}, \quad (2)$$

where  $q$  is the wave spectral index:  $q = 1$  corresponds to the flat spectrum and  $q = 5/3$  to the Kolmogorov one. The constant  $\delta B_l(k_{min})$  is scaled to match the model parameter  $\delta B \equiv [\sum_l \delta B_l^2]^{1/2}$ . Its ratio to the upstream mean magnetic field,  $\delta B/B_{0,1}$ , is our measure of the field perturbations amplitude.

The Kolmogorov wave power spectrum  $F(k) \sim k^{-5/3}$  ( $\delta B^2 = \int F(k) dk$ ) seems to be an appropriate choice for magnetic field turbulence description in real astrophysical plasmas. Such a spectrum is measured in the solar wind (Leamon et al. 1998). Interstellar scintillation observations indicate that electron density spectrum follows the Kolmogorov slope (Lee & Jokipii 1976; Lagage & Cesarsky 1983; Cho 2001; Stinebring et al. 2000) and the same character could probably be ascribed to the MHD turbulence power spectrum (Cho 2001; Cho, Lazarian, & Vishniac 2003). Such a form of the spectrum of perturbations was also often used in modeling of acceleration processes at shocks. The flat turbulence power spectrum,  $F(k) \sim k^{-1}$ , is considered here in order to check how the accelerated particle spectra depend on the value of the wave spectral index, and also to compare our results to the earlier studies. The simulations are performed for the case of a weakly ( $\delta B/B_{0,1} \ll 1$ ) and a highly ( $\delta B/B_{0,1} \gtrsim 1$ ) perturbed magnetic field. The finite-amplitude magnetic field perturbations can exist in the plasma where the shock wave propagates, as observed, e.g., for heliospheric plasma, where  $\delta B/B_{0,1} \sim 1$  (cf. Ellison et al. 1990). Calculations for nonrelativistic shocks indicate that the turbulence can be also produced upstream of the shock by nonlinear interactions between MHD waves generated by accelerated particles (Drury 1983; Lagage & Cesarsky 1983; Lucek & Bell 2000). In such a case, the resulting form of the turbulence spectrum is not satisfactorily known.

The downstream magnetic field structure is obtained from the upstream one as compressed at the shock. According to the gas compression conditions, any given point  $(x_2, y, z)$  in the downstream plasma was at the position  $(x_1 = rx_2, y, z)$  in the upstream rest frame before the shock passage. One should note that the upstream and the downstream magnetic fields are compared in two time instants, before and after the shock passage, respectively. The compression factor  $r = R\gamma_1/\gamma_2$ , where  $R$  is the shock compression ratio in the shock normal rest frame and  $\gamma_i = 1/\sqrt{1 - u_i^2}$  ( $i = 1, 2$ ). Thus, to derive the downstream field

components at the point  $(x_2, y, z)$ , we calculate the unshocked magnetic field at the point  $(x_1, y, z)$  and compress the tangential components of the magnetic field by the factor  $r$ . The field component parallel to the shock normal remains unchanged. Note that the magnetic field derived in such a way is continuous across the shock. In our approach, the shock front itself does not produce any additional fluctuations of the field. However, as pointed out by Medvedev & Loeb (1999), the relativistic two-stream instability can generate small-scale strong magnetic field perturbations in the vicinity of the shock. Thus, our modeling can be considered valid only for high-energy particles, with gyroradii much larger than the spatial scale of inhomogeneities thus generated.

## 2.2. Simulation Method

The particle equations of motion are integrated in the local (upstream or downstream) plasma rest frame, where the electric field vanishes. At the beginning of the simulation run,  $N$  monoenergetic particles (usually  $N = 100$ ) are injected at the shock front with their momentum vectors directed into the upstream region. Particle injection energy measured in the downstream rest frame is  $E_0 = 0.1$  and their resonance wave vectors  $k_{res}(E_0) \gg k_{max}$ <sup>2</sup>. After the Lorentz transformation to the upstream plasma rest frame, the trajectory of each particle is followed until it crosses the shock surface or reaches an introduced free escape boundary, located far upstream from the shock. In the latter case, the particle is assumed to escape from the acceleration region. The boundary is required to treat high-energy particles, with resonance wave vectors much smaller than  $k_{min}$ , but also the low-energy particles, with  $k_{res} \gg k_{max}$ <sup>3</sup>. Such particles are only weakly scattered by the turbulent field

---

<sup>2</sup>For superluminal shocks the seed particle injection procedure is modified. In this case, the majority of injected particles escape downstream after the first interaction with the shock and only few particles are still able to take part in the acceleration process. The resulted spectra are then determined with poor accuracy. To overcome this problem, we increase the number of injected particles in such a way to select  $N$  of those which — after transmission downstream — succeed to reach the shock front again. We have checked that the method gives the same results when applied to subluminal shocks, the only difference appears at the energy range close to  $E_0$ , which is already influenced by the initial conditions.

<sup>3</sup>The upstream escape boundary for low-energy particles with  $k_{res} \gg k_{max}$  is introduced only in the case of oblique subluminal and parallel shock waves, propagating with velocity  $u_1 = 0.5c$  in the weakly perturbed magnetic field ( $\delta B/B_{0,1} = 0.3$ ). In these cases, the upstream boundary is located at several tens of thousand of  $r_g$  ahead of the shock front. The escape boundary for energetic particles ( $k_{res} \ll k_{min}$ ) is located at 200  $r_g(E)$  ahead of the shock in the case of oblique subluminal shocks, whereas for parallel shocks it is placed at 2000  $r_g$  upstream of the shock. The number of low-energy particles escaping upstream is small. However, for highest-energy particles, with  $k_{res}(E) \ll k_{min}$ , the escape becomes efficient, leading to the formation of the cut-off in particle spectra.

and can propagate very far upstream from the shock. The upstream particles which cross the shock front are Lorentz-transformed into the downstream plasma rest frame. At this side of the shock a free escape boundary is located ‘far downstream’ from the shock at  $x_{max}(E) = X_{max} r_g(E)$  behind it. The selected value of the coefficient  $X_{max} \in (5, 150)$  depends on simulation parameters and is specified by numerical tests, separately for each shock configuration. In the conditions considered by us, very few particles are able to diffuse from such a distance back to the shock. The trajectory of a particle downstream of the shock is integrated until it crosses the escape boundary or reaches the shock front. After performing this procedure for all  $N$  particles, the first simulation cycle is finished. Then the splitting procedure is performed (see below) to replace all escaped particles with the ones still active in the acceleration process, with the respective division of the particle weights. Subsequent cycles calculations are performed analogously. The computations are finished when either more than 90% of particles escape through the introduced boundaries in an individual simulation cycle or all particles reach the upper energy boundary,  $E_{max} = 10^8$ , or the lower limit for a particle weight,  $w_{min}$  (see below), which is usually set to  $10^{-6}w_0$ . We have checked that allowing for further calculations do not noticeably influence the spectrum formed.

We use the method of trajectory splitting to derive spectra in a wide energy range (cf. Kirk & Schneider 1987b; Ostrowski 1991, 1993). At the beginning of the simulations, the same initial weight  $w_0$  is ascribed to each particle. During the calculations, some particles are lost by escaping through the boundaries. To keep the total number of particles active in the simulations constant, for each lost particle we duplicate (or multiplicate) one of those that crossed the shock upstream, with the weight of the original particle divided at equal parts between the ‘daughter’ particles. Then, we weakly perturb the motion of these particles to create different trajectories out of the splitted one. The perturbations are performed by a small change in particle positions in the shock plane,  $\Delta y, \Delta z \sim 0.0002\lambda_{min}(E)$ , where  $\lambda_{min}(E)$  is the smallest scale of the resonant range of the field perturbations, defined in Section 2.3. For the splitting procedure we take particles with the highest weights and smallest energies available. With this method, the effective number of particles in the simulation is much higher than the injected number, and a particle spectrum is determined with approximately the same accuracy at all energies.

A spectrum of accelerated particles and their angular distribution are measured at the shock, in the shock rest frame. Every time a particle crosses the shock front, a value  $w/(|v_x| + 0.005)$  is added to the respective logarithmic energy bin and to the respective  $\cos\theta$  bin.  $\theta$  is the angle between the particle momentum and the shock normal (note that  $\theta$  is not the pitch-angle measured with respect to the mean magnetic field),  $v_x$  is a normal component of the particle velocity and  $w$  is its weight. The weighting factor  $(|v_x| + 0.005)$  is needed to

transform the particle flux into the particle density (cf. Kirk & Schneider 1987b) and the additional term 0.005 ensures the proper behavior near  $v_x = 0$ . The spectra and angular distributions presented are averaged ones over a few (usually 10) different sets of  $N$  particles and realizations of the perturbed magnetic field.

### 2.3. Derivation of Particle Trajectories

The particle orbits are calculated using the Runge-Kutta 5-th order method with the adaptive stepsize control (routine RKQS in: Press et al. 1992). This routine allows for an accurate derivation of particle trajectories in a turbulent magnetic field with the optimized simulation time (see also Appendix B). However, the procedure becomes very time consuming for higher-energy particles, because exact derivation of a trajectory with short wave perturbations requires extremely short time-steps (in units of  $r_g/c$ ) to be used. At the same time, the considered short waves, with  $\lambda \ll r_g$ , only weakly influence trajectories of such particles. Therefore, in our modeling the motion of a higher-energy particle is derived within the proposed hybrid approach. It involves exact integration of particle trajectories in the turbulent field including long and resonance waves ( $\lambda > \lambda_{min} = 0.05r_g(B = B_{0,1})$ )<sup>4</sup> and the short wave influence on the trajectory is included as a respective small amplitude momentum scattering term. A scattering probability distribution is determined by additional simulations, involving the full set of the short waves considered (see Appendix A).

### 2.4. Tests

A number of tests have been performed on the simulation code. Some of them have been mentioned in the preceeding subsections, the others are described in detail in Appendix B.

## 3. RESULTS

Our Monte Carlo simulations of the first-order Fermi acceleration process have been performed in order to study a role of the applied magnetic field structures for the test particle acceleration at relativistic shocks. Because of the limited dynamic range of field

---

<sup>4</sup>The short waves downstream of the shock are defined by a particle gyroradius in the upstream mean magnetic field  $B_{0,1}$ . However, this assumption does not influences the particle spectra formed, as discussed in Appendix B.

perturbations, scattering conditions vary with increasing particle energies. We study how this influences the particle spectrum formation and how the spectra depend on the shock velocity and on the parameters of the magnetic field: the mean field inclination and the spectrum of finite-amplitude perturbations. In the case of oblique subluminal shocks, the accelerated particle spectral index can vary with the turbulence amplitude. At superluminal shocks, the presence of finite-amplitude perturbations near the shock plays an essential role for particle acceleration. In weakly scattering conditions, the first-order Fermi process is inefficient in such shocks and particles can gain energies only by the one way compression at the shock (Begelman & Kirk 1990). Formation of power-law spectra is possible for larger amplitudes of the magnetic field perturbations. In particular, we discuss the role of long wave perturbations, which lead to the formation of locally oblique subluminal configurations at the shock. In the conditions provided, the energy gains of particles interacting with the shock can increase and particle reflections from the respective regions of the compressed field downstream of the shock may occur. The importance of this factor on the particle spectra formation is investigated for parallel shocks as well.

Accelerated particle spectra formed at oblique shock waves are presented in Figure 1 for the case of subluminal magnetic field configuration, and in Figures 4 and 8 for superluminal shocks. Particle spectra derived for parallel shocks are shown in Figure 9. The particle spectra were calculated for three different upstream magnetic field perturbation amplitudes  $\delta B/B_{0,1} = 0.3, 1.0$  and  $3.0$ , referred to below as the ‘small’, ‘medium’ and ‘large’ (‘high’) amplitude perturbations, respectively. The amplitudes  $\delta B/B_{0,1}$  are indicated in the figures near the respective curves. Spectra for different  $\delta B/B_{0,1}$  are not normalized, they have vertical shifts for presentation clarity. Linear fits to the power-law parts of the spectra are also presented in the figures and values of the spectral indices  $\alpha$  are given. Accuracies of the presented fits are usually better than  $0.02$  in  $\alpha$  for subluminal and parallel shocks, with some exceptions discussed in the following. For superluminal shocks, the evaluated statistical errors  $\Delta\alpha \approx 0.03 - 0.06$ . One should note that the power-law character of some particle spectra is only approximate because of the existing spectrum curvature (see, e.g., Figures 4d,f and 8b) and thus the value of the spectral index derived depends also directly on an energy range chosen for the fit. The narrow energy range values of  $\alpha$ , indicated in Figures 4 and 8, are shown for comparison to the spectral indices of the other spectra presented.

Particles in the energy range indicated in the figures by arrows above the horizontal energy axis can effectively interact with the magnetic field inhomogeneities, due to the resonant condition satisfied,  $k_{min} \lesssim k_{res} \lesssim k_{max}$  ( $k_{res} \equiv 2\pi/r_g$ ). The limits are not precise, they are calculated for the upstream magnetic field strength  $B_{0,1} = 1$  and particle transverse momenta  $p_\perp = p$ . The particle energies considered in the simulations can be scaled to various shock conditions by the respective identifications of  $B_{0,1}$ ,  $\psi_1$ ,  $\delta B$ ,  $k_{min}$  and  $k_{max}$ .

### 3.1. Oblique Subluminal Shock Waves

To illustrate the characteristic features of particle acceleration processes at relativistic oblique subluminal ( $u_1/\cos\psi_1 < c$ ) shocks, we have studied the shock wave propagating with velocity  $u_1 = 0.5c$  ( $\gamma_1 \simeq 1.2$ ) into the upstream plasma with the mean magnetic field inclined to the shock normal at  $\psi_1 = 45^\circ$ . The shock velocity along the mean magnetic field is then  $u_{B,1} \simeq 0.71c$ . Figure 1 shows accelerated particle spectra, derived in the shock rest frame, for the flat and the Kolmogorov wave power spectrum. One may note that the particle spectra diverge from a power-law in the full energy range. Usually a harder spectral component appears at highest energies, followed by the spectrum cut-off. The shape of the particle spectrum depends on both the amplitude of the magnetic field perturbations and the spectral index of the wave power spectrum.

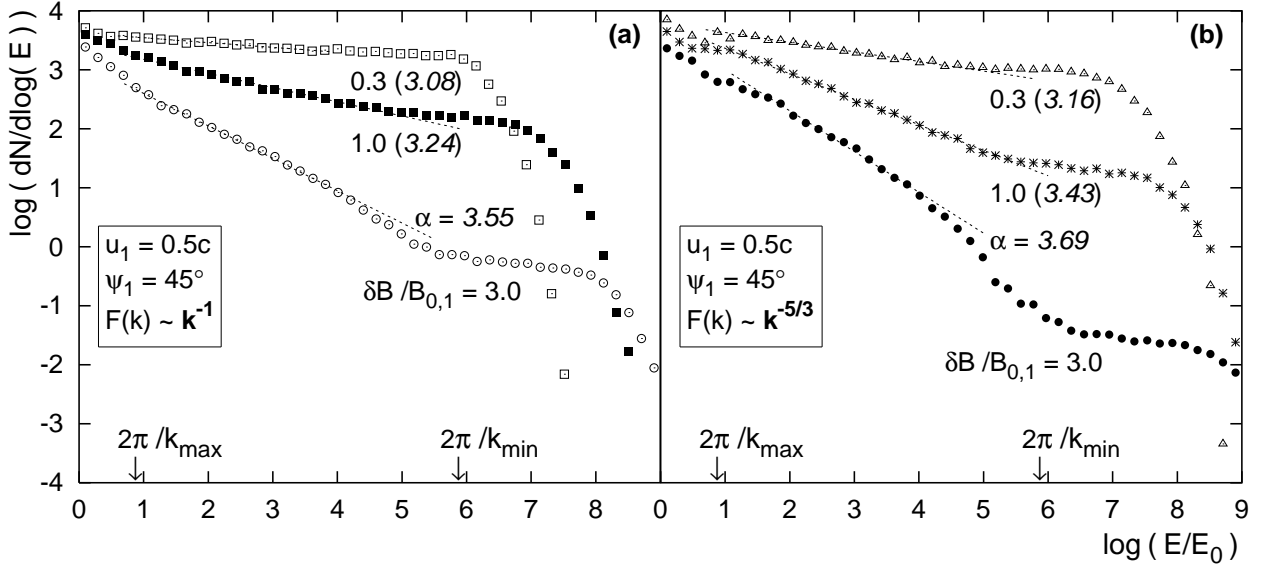


Fig. 1.— Particle spectra at the subluminal shock wave ( $u_1 = 0.5c$ ,  $\psi_1 = 45^\circ$  and  $u_{B,1} \simeq 0.71c$ ) for the flat (a) and the Kolmogorov (b) wave spectrum of magnetic field perturbations. Any individual point in the spectrum represents a particle number (weight)  $dN$  recorded per a logarithmic energy bin. The upstream perturbation amplitude  $\delta B/B_{0,1}$  is given near the respective results. Linear fits to the spectra are also presented and values of the spectral indices  $\alpha$  are given in italic. The spectra have vertical shifts for clarity. Particles with energies in the range  $(2\pi/k_{max}, 2\pi/k_{min})$  indicated by arrows can effectively interact with the magnetic field inhomogeneities.

A power-law part of the particle spectrum steepens with the increasing amplitude of the field perturbations for the three cases considered. For the flat turbulence spectrum,

the particle spectrum is very flat ( $\alpha \approx 3.08$ ) for the weakly perturbed field  $\delta B/B_{0,1} = 0.3$ . For larger perturbation amplitudes we have  $\alpha \approx 3.24$  and  $\alpha \approx 3.55$  for  $\delta B/B_{0,1} = 1.0$  and 3.0, respectively. The spectral indices obtained are consistent with previous numerical calculations of Ostrowski (1991, 1993) and, in the limit of small perturbations, with the analytic results obtained by Kirk & Heavens (1989).

Variations of the accelerated particle spectral index with the turbulence amplitude, for a given mean field inclination, was discussed by Ostrowski (1991). As already mentioned in Section 1, in a weakly perturbed magnetic field there is a high probability of reflection of upstream particles from the compressed field behind the shock. The repeating particle reflections lead to the formation of a very flat energy spectrum. When the perturbation amplitude increases, the reflection probability is diminished and the mean energy gains of particles interacting with the shock decrease. At the same time, the escape probability for downstream particles decreases, as the field perturbations enable particles to diffuse across the field lines. However, this reduction of the escape probability is slow, so that increased upstream-downstream transmission probability leads to the net more efficient particle escape and the resulting steepening of the spectrum.

The differences in the particle spectra obtained for the Kolmogorov and the flat wave power spectrum are clearly visible from comparison of Figures 1a and 1b. In particular, for a given  $\delta B/B_{0,1}$ , the power-law part of the spectrum is steeper for the Kolmogorov wave spectrum and the final hardenings of the spectra are more pronounced in this case.

The non-power-law character of the particle spectra obtained results from the limited dynamic range of the magnetic field perturbations. In the energy range where an approximate power-law spectrum forms, particles are effectively scattered by the resonant magnetic field inhomogeneities. The character of the spectrum changes at high particle energies, for which resonance wave vectors  $k_{res} \lesssim k_{min}$ . These particles interact with the magnetic field perturbations being the short wave turbulence and are only weakly scattered. Thus, analogously to weakly scattering conditions, the anisotropically distributed upstream particles can be effectively reflected from the region of the compressed magnetic field downstream of the shock, leading to the spectrum flattening. The effectiveness of reflections and the resulting modification of the spectrum depend on the amplitude and the spectrum of field perturbations, as can be seen in the figures. Finally, a cut-off in the spectrum appears due to weakly scattered particles escaping through the introduced upstream boundary.

Effects of the finite wave vector range can be also observed for particles within the resonance range,  $k_{min} \lesssim k_{res} \lesssim k_{max}$ , for the magnetic field perturbations considered. The change of the scattering conditions with the increasing particle energies should lead to the modest but continuous variation of the particle spectral slope. The effect is visible (Figure 2)

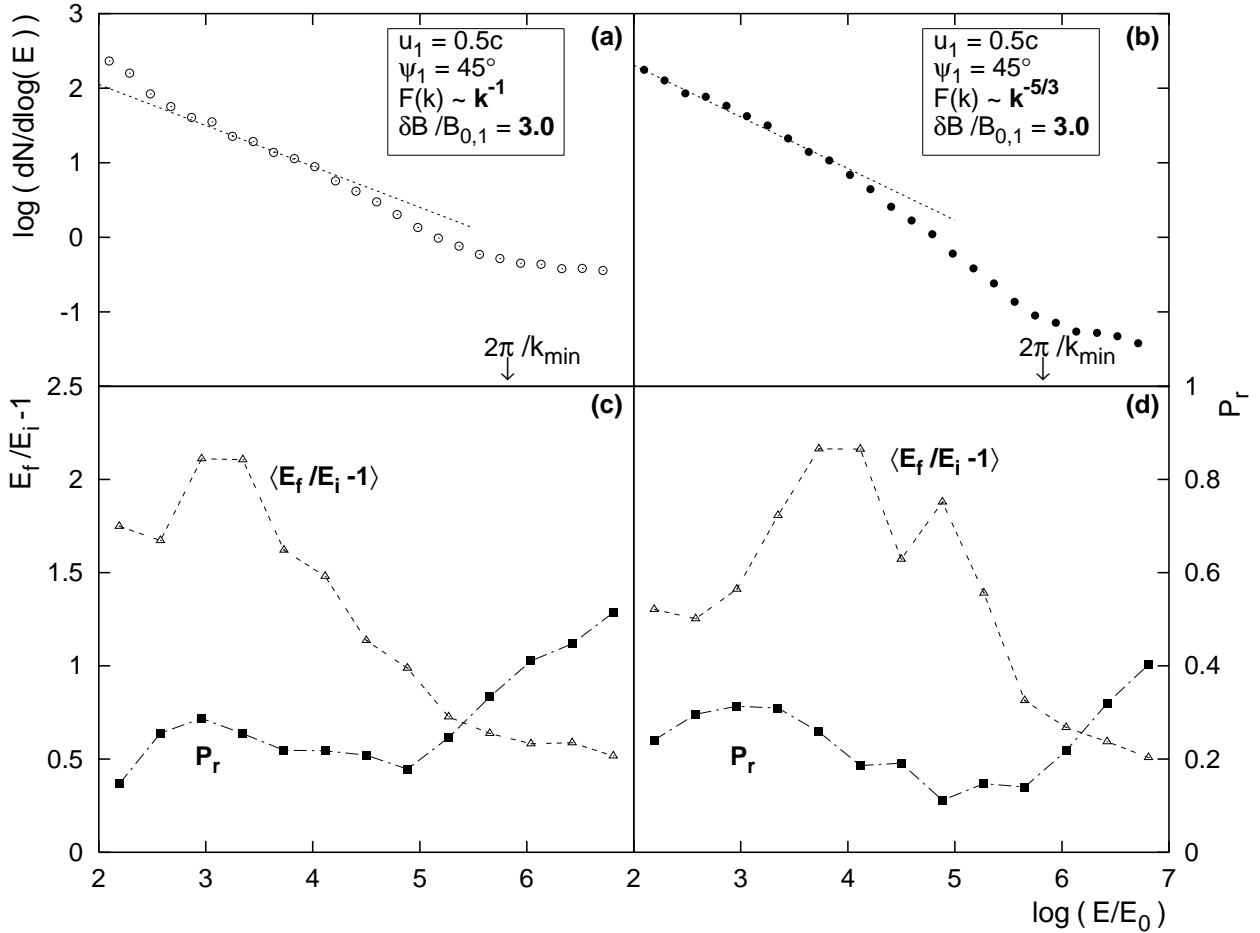


Fig. 2.— Probability of particle reflection  $P_r$  and the mean energy gain of reflected particles  $\langle E_f/E_i - 1 \rangle$  in the energy range where the particle spectrum deviates from a power-law form. The respective parts of particle spectra are shown in the upper panels. Power-law fits are the same as shown in Fig. 1. The values of  $P_r$  and  $\langle E_f/E_i - 1 \rangle$  were obtained in additional simulations, with the particle injection energy  $E = 10$ , so that the first few points are influenced by the initial conditions. In this figure, the energies  $E_i$  and  $E_f$  are measured in the upstream plasma rest frame and the particle spectra are calculated also in this frame. To limit statistical fluctuations, the logarithmic energy bin used in lower panels is twice as large as the respective bins in the upper panels. The respective upstream-downstream transmission probability  $P_{12} = 1 - P_r$ .

for the case of a highly turbulent magnetic field  $\delta B/B_{0,1} = 3.0$ . The noticeable steepening of the spectrum for particle energies  $\log(E/E_0) \gtrsim 4$  is accompanied by a slow decrease of the probability of reflection,  $P_r$ , and the mean energy gain at an individual particle-shock interaction (Figures 2c,d; for the probability of reflection and the mean energy gains calculations see Section 3.4). At higher energies,  $P_r$  starts to grow again, without any increase in  $\langle E_f/E_i - 1 \rangle$ , which results in a harder spectrum. Thus, the main factor leading to the variation of a spectrum inclination is the increased upstream particle transmission probability and thus the increased escape probability. The decrease in  $P_r$  and in the mean energy gain of reflected particles stems possibly from the fact that for high-energy particles (but still with  $k_{res} \gtrsim k_{min}$ ) there are gradually fewer large amplitude long wave magnetic field perturbations for an increasing particle energy and, therefore, the effective mean inclination of the magnetic field at the shock decreases, leading to the effects discussed. These effects are not visible in the spectra for smaller  $\delta B/B_{0,1}$  since the amplitudes of long wave perturbations are moderate in these cases. In the case of the Kolmogorov wave power spectrum yet another effects might be responsible for the decrease in the reflection probability. The first factor is related to the increasing amplitude of the resonant perturbations with the increasing particle energy, leading to a gradual breakdown of approximate magnetic moment conservation. At the same time, the perturbation amplitude growth leads to additional isotropization of particles hitting the shock from upstream. This increases the mean inclination of particle momenta crossing the shock, increasing the mean energy gain of a few reflected particles and increases the particle upstream-downstream transmission probability (cf. Ostrowski 2002). The effect can be also visible for particles forming the power-law part of the spectrum. As Figures 2b,d show, the mean energy gain grows with energy for these particles, the feature not observed with the flat wave power spectrum (Figures 2a,c).

Example particle angular distributions at the shock are presented in Figure 3 for particles forming the power-law part of the energy spectrum and for particles responsible for the flatter high-energy spectral component. Anisotropies of the distributions presented for the power-law parts of the particle spectra are larger in the case of the Kolmogorov wave power spectrum. Angular distributions for particles forming the harder spectral component hardly depend on the wave power spectrum.

### 3.2. Oblique Superluminal Shock Waves

Spectra for superluminal shocks are presented in Figure 4 for a number of the mean magnetic field configurations, and shock velocities (Lorentz factors)  $u_1 = 0.5c$  ( $\gamma_1 \simeq 1.2$ ) and  $u_1 = 0.9c$  ( $\gamma_1 \simeq 2.3$ ). For the inclination angle  $\psi_1 = 75^\circ$  considered, the shock wave

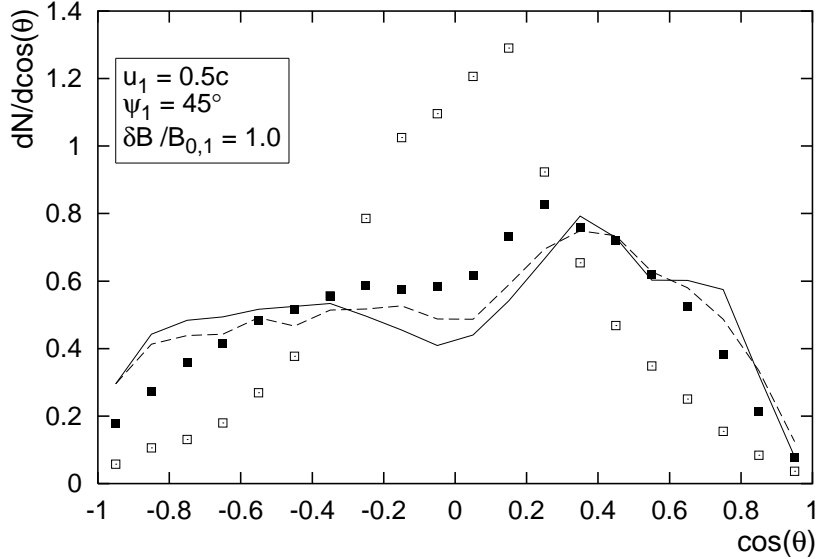


Fig. 3.— Particle angular distributions at the shock front for  $\delta B/B_{0,1} = 1.0$ , in the shock rest frame. The angular distributions for particles forming the power-law part of the energy spectrum,  $1 \leq \log(E/E_0) \leq 5$ , are shown by the filled and open squares for the flat and the Kolmogorov wave power spectrum, respectively. Angular distributions for particles responsible for the harder spectral component,  $5 \leq \log(E/E_0) \leq 7$ , are presented by the solid (flat spectrum) and dashed (Kolmogorov spectrum) lines. All distributions are normalized to the unit surface area under the respective curves. Particles with  $\cos \theta < 0$  are directed upstream of the shock.

propagation velocity along the mean magnetic field component is  $u_{B,1} \simeq 1.93c$  for  $u_1 = 0.5c$  and  $u_{B,1} \simeq 3.48c$  for  $u_1 = 0.9c$ . For the smaller  $\psi_1 = 45^\circ$  and the shock velocity  $u_1 = 0.9c$ , the projected velocity  $u_{B,1} \simeq 1.27c$ .

For the small turbulence amplitude ( $\delta B/B_{0,1} = 0.3$ ) in all cases studied, we approximately reproduce results of Begelman & Kirk (1990), showing a ‘super-adiabatic’ compression of injected particles, but hardly any or an extremely steep power-law spectral tail. However, our method of particle injection does not match initial conditions of the compression process, which takes place when the initially isotropically distributed particles cross the shock. Because of this, in order to directly estimate the role of this process on particle spectrum formation, additional simulations have been performed. In these simulations, a set of  $N = 20000$  particles with energy  $E_{0,1} = E_0$  was injected  $10 r_{g,1}$  in front of the shock with the isotropic angular distribution in the upstream plasma rest frame. In these simulations we studied the shock wave propagating with velocity  $u_1 = 0.5c$  in the plasma with the magnetic field composed of the regular component only ( $\delta B/B_{0,1} \equiv 0$ ) inclined at the angle  $\psi_1 = 45^\circ$

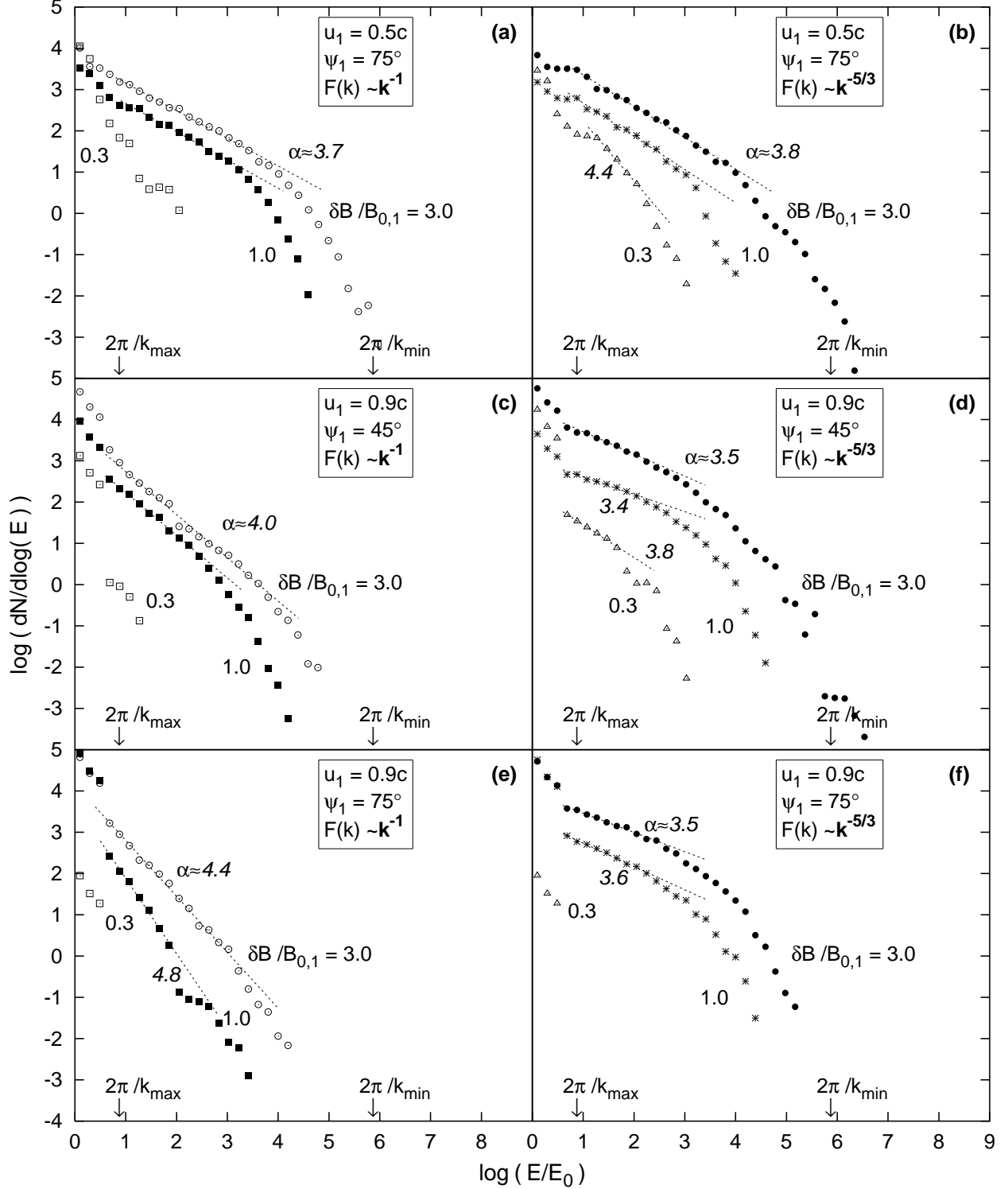


Fig. 4.— Accelerated particle spectra at oblique superluminal shocks with  $u_1 = 0.5c$  and  $u_1 = 0.9c$ . Parameters for each spectrum are provided in the respective panels.

to the shock normal (cf. Figures 4a,b). Therefore, in the absence of scattering, the particle energy gains are solely due to the acceleration at individual shock transmissions. The trajectory of each injected particle was followed until, after interacting with the shock surface, it reached the free escape boundary located  $30 r_{g,2}$  downstream of the shock. Note that an interaction with the shock wave may involve a number of particle trajectory crossings of the shock front. The resulting particle spectrum is shown in Figure 5 (filled squares), where the spectra formed in the weakly perturbed magnetic field  $\delta B/B_{0,1} = 0.3$  are also presented for comparison. These spectra were calculated using the above described method, with particle injection upstream of the shock. One can see that the presence of small amplitude magnetic field perturbations hardly influences the particle spectrum formation. The spectrum is essentially the ‘super-adiabatically’ compressed initial one and the power-law part, with a sharp cut-off at  $E \sim 10^2 E_0$ , is formed by a few particles only. The energetic tail generation is due to locally subluminal magnetic field configurations formed at the shock front, which enable particle reflections or extended interaction with the shock. As the locally subluminal field configurations are produced mainly by high amplitude long wave perturbations,

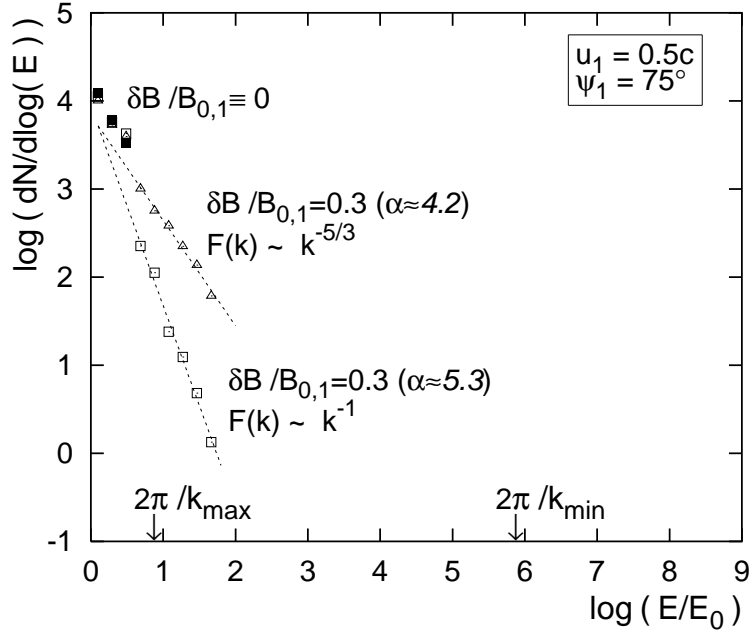


Fig. 5.— Compressed particle spectra at the superluminal shock with  $u_{B,1} \simeq 1.93c$ . The results for  $\delta B/B_{0,1} \equiv 0$  are presented by filled squares. The presence of small amplitude magnetic field perturbations,  $\delta B/B_{0,1} = 0.3$ , produces power-law tails, as illustrated by the spectra obtained for the flat (open squares) and the Kolmogorov (open triangles) wave power spectra. The spectra presented are normalized in a way to have the same particle weight in each spectrum.

these processes are more efficient for the Kolmogorov-type field perturbations. Therefore, the power-law part of the particle spectrum is flatter in this case, when compared to the spectrum for the flat wave power spectrum. Modifications of the compression process due to the presence of the magnetic field perturbations depend on the shock velocity and on the mean field configuration, as one can see from Figure 4 (cf. also Ostrowski 1993). For lower  $u_{B,1} > 1$ , the weakly perturbed magnetic field can modify the spectra, whereas for highly superluminal configurations the power-law part is not generated for  $\delta B/B_{0,1} = 0.3$  (Figures 4e,f). At larger turbulence amplitudes power-law sections in the spectra are again produced in the limited energy ranges. The spectral indices vary with varying conditions at the shock, including the shock velocity, the mean field inclination, the amplitude and the spectrum of magnetic field perturbations. The steepening and the cut-off occur at low energies, in the resonance range, contrary to the subluminal shocks at the same turbulence amplitudes.

The spectrum steepening and the cut-off in the resonance energy range are related to the character of the first-order Fermi process at superluminal shocks, in conditions of a highly perturbed magnetic field near the shock. The presence of 3D, finite-amplitude magnetic field perturbations enables efficient particle cross-field diffusion (e.g., Gaicalone & Jokipii 1994), but also leads to the formation of locally oblique, subluminal field configurations at the shock front. Such configurations are formed by long wave high amplitude magnetic field perturbations and enable particle interactions with the shock in locally subluminal conditions. In some cases reflections from compressed downstream fields can also occur. In effect, the energy gains of particles interacting with the shock in the locally subluminal conditions can be much larger than of those interacting within the locally superluminal field configurations. The role of this factor in forming particle spectra was originally discussed by Ostrowski (1993). For the sufficiently high turbulence amplitude he obtained power-law spectra in a wide energy range due to similar scattering conditions at each particle energy. In our present simulations, because of the limited wave vector range, the scattering conditions vary with a particle energy, leading to the spectral features which have not been discussed so far. Figure 6 shows a variation of the particle reflection probability with the particle energy for the shock wave with  $u_1 = 0.9c$  and  $\psi_1 = 45^\circ$ . We use this parameter to describe subluminal features of the acceleration process. Note, however, that it is not only reflections what is responsible for the observed changes in the acceleration process — variations of the mean energy gain at the particle-shock interaction and of the downstream particle escape rate can also play a role. As shown in Figure 6, in the energy range where a power-law part of the spectrum forms, the reflection probability changes slightly, as particle resonance wave vectors are much larger than  $k_{min}$ . Since at a given  $\delta B/B_{0,1}$  the amplitudes of long wave magnetic field perturbations are larger for the Kolmogorov turbulence,  $P_r$  is greater in this case. When the reflection probability starts to decrease, the particle spectrum steepens

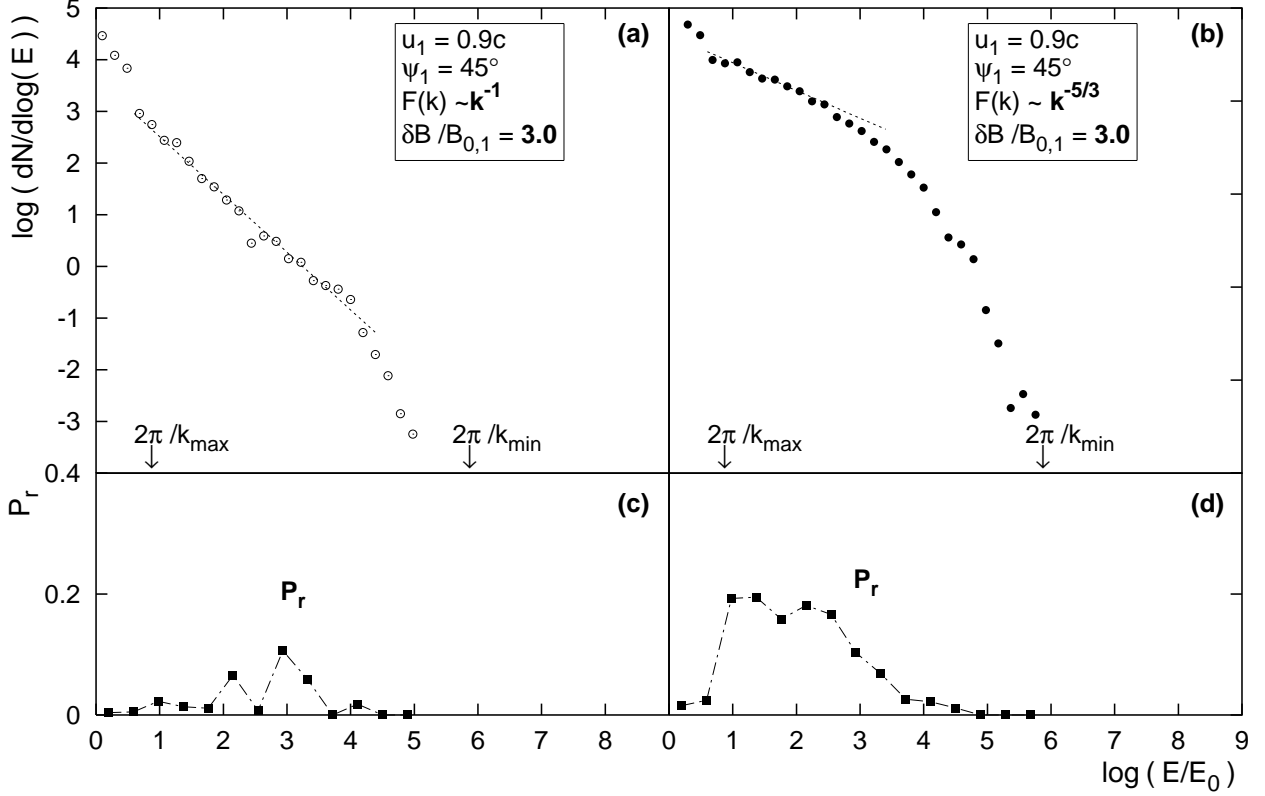


Fig. 6.— Particle spectra at the superluminal shock wave with parameters given in the panels. In lower panels the respective particle reflection probability is provided. The spectra presented correspond to those shown in Figs. 4c,d for the case of  $\delta B/B_{0,1} = 3.0$ .

and, finally, for  $P_r \simeq 0$ , the cut-off occurs. At least two factors can be responsible for the decrease of  $P_r$ . The first one is related to the limited dynamic range of the field perturbations — with increasing particle energy there are gradually less respective long waves and most of particles meet effectively superluminal conditions at the shock. The second factor is due to accompanying increase of the resonant perturbations amplitude for the Kolmogorov spectrum, as discussed in Section 3.1.

Examples of particle angular distributions derived at the superluminal shock are presented in Figure 7 for the case of the highly perturbed magnetic field  $\delta B/B_{0,1} = 3.0$ .

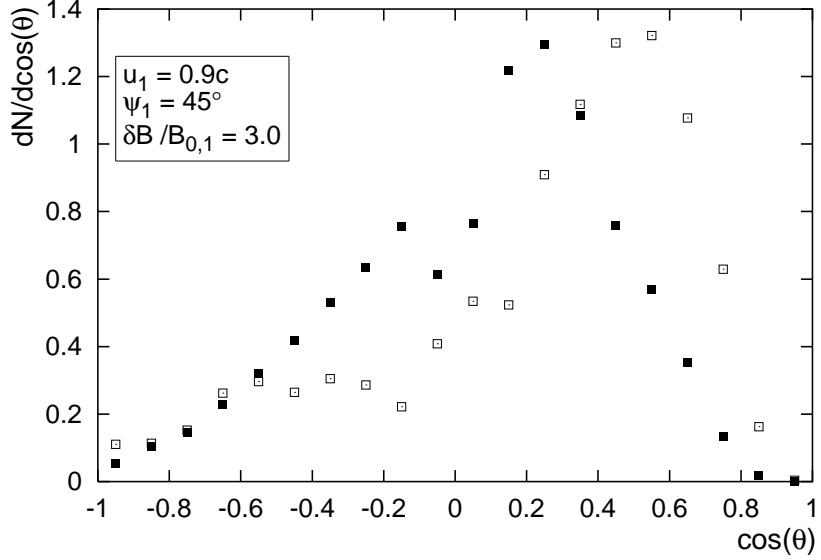


Fig. 7.— Particle angular distributions at the superluminal shock wave for  $\delta B / B_{0,1} = 3.0$  in the shock rest frame. The angular distributions are formed by particles with energies in the range  $1 \leq \log(E/E_0) \leq 5$  and are shown by the filled and open squares for the Kolmogorov and the flat wave power spectrum, respectively.

### 3.3. High $\gamma$ Shock Waves

Particle spectra at the shock wave propagating with velocity  $u_1 = 0.98c$  into the magnetic field with the mean field inclined at the angle  $\psi_1 = 45^\circ$  are presented in Figure 8. The shock Lorentz factor is  $\gamma_1 \simeq 5$ , so one can consider the shock as the ultrarelativistic one. As can be seen in the figure, the main particle acceleration process in this case is the particle compression at the shock — the power-law tail is formed by only a small fraction of injected particles, in the case of a highly perturbed magnetic field. For the flat wave power spectrum the power-law part is very steep,  $\alpha \approx 7$ , for the Kolmogorov turbulence  $\alpha \approx 3.9$  with accuracy  $\Delta\alpha \sim 0.1$ . The spectrum cut-off occurs well in the resonance energy range, at lower energies in comparison to the lower  $\gamma$  shocks. This feature is independent of the initial energy of particles injected at the shock, as illustrated by the particle spectra calculated for the other injection energies<sup>5</sup>. It seems therefore that it is the turbulent magnetic field struc-

<sup>5</sup>The average magnetic field strength  $\langle (B_0 + \delta B)^2 \rangle^{1/2}$  downstream of the shock is  $\langle B_2 \rangle \approx 30B_{0,1}$  and the wave vectors of magnitude  $k_{max}$  are the resonance ones for the particles of energies  $E \approx 2\pi\langle B_2 \rangle / k_{max} \approx 18.8$ . Simulations for the other injection energies have been performed in order to check if the cut-off occurring in the particle spectra is not due to the particle injection procedure applied. For the particle injection energy  $\log(E/E_0) = 2$  this procedure gives the respective wave vectors  $k_{res} = 2\pi/r_g(B = \langle B_2 \rangle) \lesssim k_{max}$  (cf.

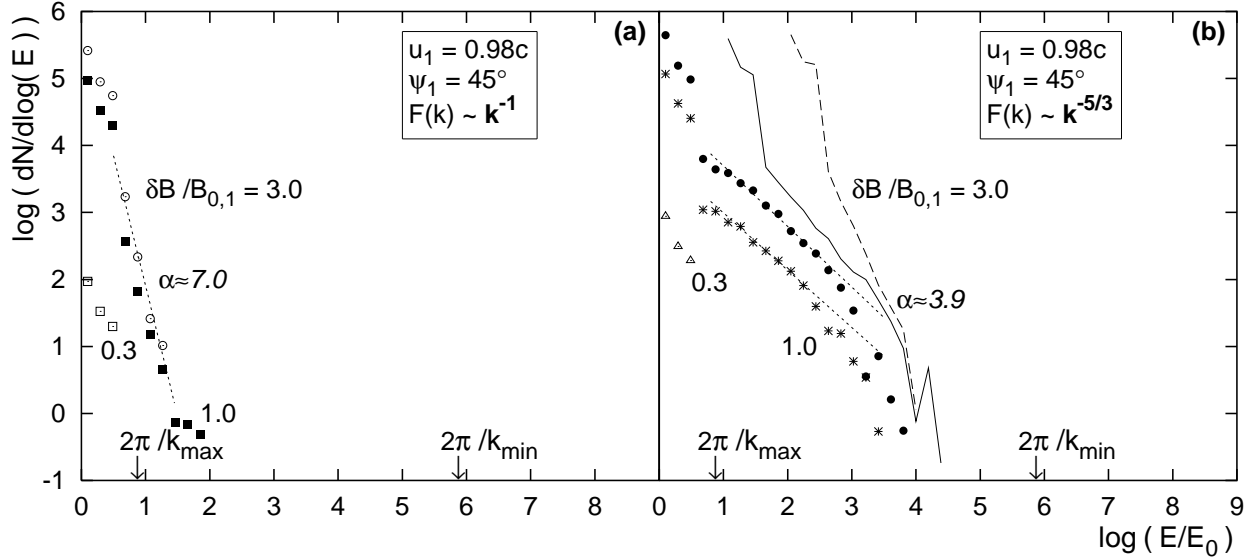


Fig. 8.— Accelerated particle spectra at the ultrarelativistic shock wave ( $u_1 = 0.98c$ ,  $\gamma_1 \simeq 5$ ). In panel (b) the particle spectra obtained for higher particle injection energies,  $E_{inj}$ , are presented by the solid and the dashed line for  $\log(E_{inj}/E_0) = 1$  and  $\log(E_{inj}/E_0) = 2$  ( $\delta B/B_{0,1} = 3.0$ ), respectively.

ture which becomes effectively perpendicular and does not allow for particle acceleration to higher energies. Note however, that the  $\gamma_1 \simeq 5$  case we analyzed was at the limit of the application range of our simulation method. Thus this attempt at studying the first-order Fermi process at ultrarelativistic shock waves should be treated with some caution.

### 3.4. Parallel Shock Waves

As discussed by Ostrowski (1988b) for nonrelativistic shocks, the presence of finite-amplitude magnetic field perturbations modifies character of diffusive particle acceleration at shock waves with the mean field parallel to the shock normal. The effect arises due to locally oblique field configurations, formed by long wave perturbations at the shock front and the respective magnetic field compressions downstream of the shock. As a result, the mean particle energy gains may increase and the particles reflected from the shock front can occur. The analogous phenomena should occur at relativistic shocks (cf. Ostrowski 1993).

In the numerical simulations of Bednarz & Ostrowski (1996) of the first-order Fermi

---

Section 2.2).

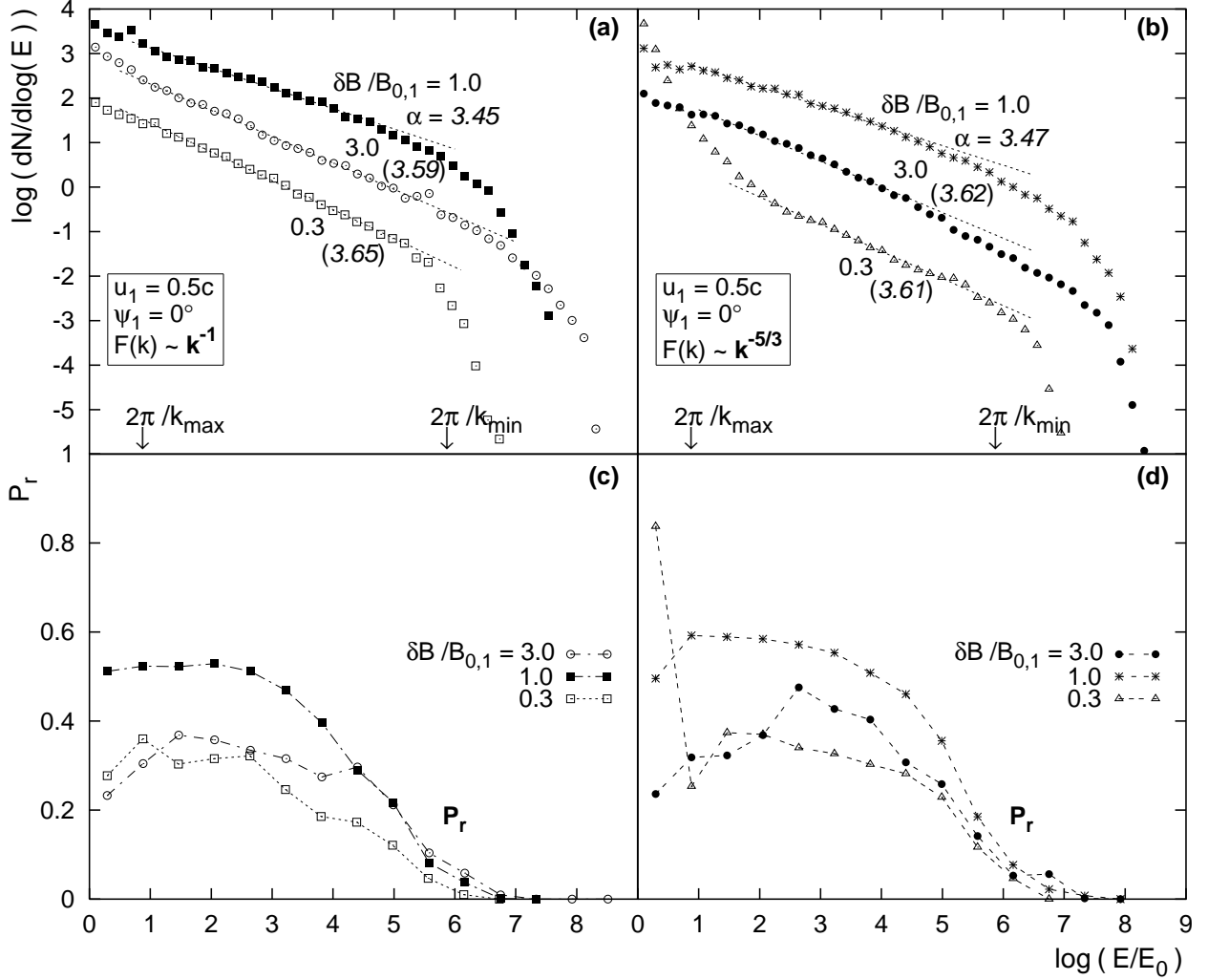


Fig. 9.— Accelerated particle spectra at the parallel shock wave with  $u_1 = 0.5c$ . For upstream particles, probability of reflection from the shock,  $P_r$ , is presented as a function of a particle energy for the respective particle spectra above.

acceleration at parallel mildly relativistic shocks, the acceleration time scale reduces with increasing turbulence level, but no spectral index variation is observed. The same behavior occurs for parallel ultrarelativistic shocks, where the value of the spectral index for a given shock velocity is independent of the magnetic field perturbation amplitude (Bednarz & Ostrowski 1998). However, the considered acceleration models apply very simple modeling of the perturbed magnetic field effects by introducing particle pitch-angle scattering. Such an approach does not allow for studying effects of long wave perturbations. We therefore decided to investigate such processes with the ‘realistic’ magnetic field turbulence model

applied in the present simulations.

In Figure 9 we present particle spectra for the mildly relativistic parallel shock wave with  $u_1 = 0.5c$ . The spectral indices fitted to the power-law parts of the spectra are listed below in Table 1. One can note that the particle spectral indices deviate from the small amplitude results of the pitch-angle diffusion model — the values of  $\alpha$  calculated by Heavens & Drury (1988) are also presented in the table. In addition, increasing magnetic field perturbations produce non-monotonic changes of the particle spectral index — the feature which has not been discussed for parallel shocks so far. Analogously to oblique shock waves, our particle spectra are non-power-law ones in a full energy range, and the shape of a spectrum vary with the amplitude of turbulence and the wave power spectrum.

The non-monotonic variation of the spectral index with the turbulence amplitude results from modifications of the particle acceleration process at the shock. The long wave finite-amplitude perturbations produce locally oblique magnetic field configurations and lead to the occurrence of, e.g., particles reflected from the compressed field downstream of the shock. In order to quantitatively estimate effects of such locally oblique field configurations on the particle spectrum formation, we calculated the mean reflection rate and the mean energy gains of particles interacting with the shock. We used the following method (cf. Ostrowski 1988b). The process of an upstream particle interaction with the shock begins when it crosses the shock front downstream for the first time. A given particle is assumed to continue its interaction with the shock if, after crossing the shock, it reaches the shock front again not later than  $1.1t_{g,max}$  and, at the same time, its distance from the shock does not exceed  $2r_{g,max}$ . The particle gyration time  $t_{g,max}$  and the gyroradius  $r_{g,max}$  are derived for the average magnetic field  $\langle(\mathbf{B}_0 + \delta\mathbf{B})^2\rangle^{1/2}$  in the respective local plasma rest frame. A particle trajectory is integrated, including possible successive shock crossings, until it exceeds one of temporal or spatial barriers thus defined. When it takes place downstream of the shock, the particle is counted as the transmitted one. If it occurs upstream, the particle is assumed to be the reflected one. A reflected particle starts its new interaction when it encounters the shock front again. A transmitted particle, after moving in the perturbed magnetic field, is sometime able to recross the shock again upstream and to start its new interaction with the shock. For each reflected or transmitted particle, its weight  $w$ , the final,  $E_f$ , and the initial,  $E_i$ , energy are measured, the last quantity derived in the upstream plasma rest frame at the first particle shock crossing. In order to calculate the reflection,  $P_r$ , and the transmission,  $P_{12}$ , probability, a particle weight is added to the respective logarithmic energy  $E_i$  bin for the reflected particles ( $S_r$ ) and the transmitted ones ( $S_{12}$ ). Then, the reflection probability is calculated as  $P_r = S_r/(S_r + S_{12})$  and, analogously,  $P_{12} = S_{12}/(S_r + S_{12})$ . The particle energy gains are derived as  $(E_f - E_i)/E_i$ ;  $E_f$  for the transmitted particles being calculated in the downstream plasma rest frame (cf. Ostrowski 1988a).

Reflection probability in function of particle energy is presented in Figures 9c,d for the respective particle spectra shown in upper panels. As one can note, the probability of reflection depends on the turbulence amplitude and the amount of field perturbations with wavelengths larger than the resonance wavelength for a given particle. For  $\delta B/B_{0,1} = 1.0$  the reflection probability is higher as compared to the other perturbation amplitudes considered, and the resulting particle spectrum is flatter. For the chosen by us  $\delta B/B_{0,1} = 0.3$  and 3.0 the values of  $P_r$  (and  $P_{12} = 1 - P_r$ ) do not differ considerably, which results in similar particle spectral indices. One can note that the spectra obtained for the Kolmogorov case seem to exhibit a continuous slow steepening. Thus, the fitted power-laws depend to some extent on an energy range chosen for the fit, with accompanying variations of  $\alpha$  reaching  $\Delta\alpha \sim 0.04$ . One can also note a steep part of the spectrum at low energies for  $\delta B/B_{0,1} = 0.3$  in Figure 9b. This is due to weak resonant scattering of low-energy particles, escaping thus along the magnetic field lines through the upstream free escape boundary, located 30000  $r_g$  from the shock.

The presented reflection probabilities decrease at high particle energies due to a limited dynamic range of the magnetic field turbulence. The locally oblique field configurations are mainly formed by long wave perturbations ( $k \ll k_{res}$ ) (cf. Ostrowski 1988b). For high energy particles with  $k_{res} < k_{min}$  there are no such long waves and the upstream particles can be

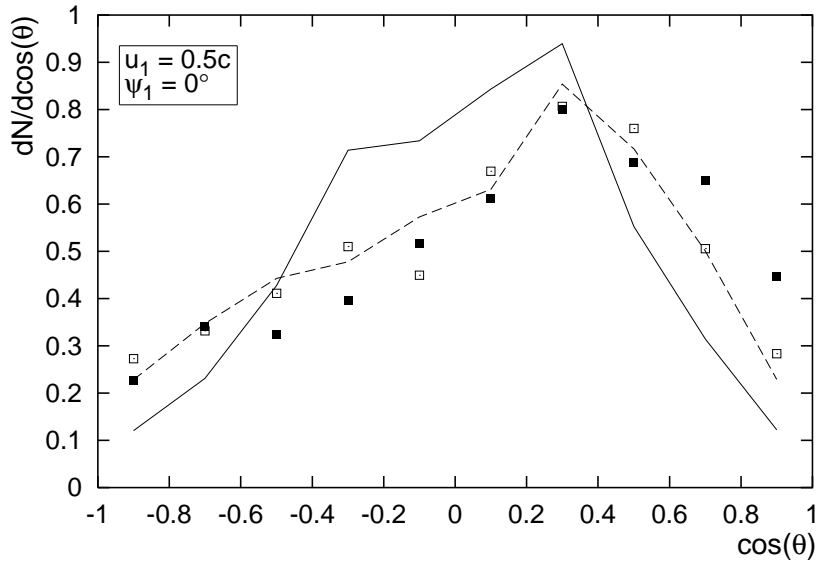


Fig. 10.— Particle angular distributions at the parallel shock wave with  $u_1 = 0.5c$  formed by particles with energies in the range  $1 \leq \log(E/E_0) \leq 5$  for the small ( $\delta B/B_{0,1} = 0.3$ , squares) and the large ( $\delta B/B_{0,1} = 3.0$ , lines) turbulence amplitude. Open squares and the dashed line are for  $F(k) \sim k^{-1}$ ; filled squares and the solid line for  $F(k) \sim k^{-5/3}$ .

only transmitted downstream of the shock. In these conditions, the acceleration process should converge to the ‘classic’ parallel shock acceleration model, but in our simulations particles can move far to the introduced escape boundary at  $x_{max} = 120r_g(E)$ , forming a cut-off.

Figure 10 shows particle angular distributions for particles forming power-law parts of the energy spectra. For the small amplitude of magnetic field perturbations,  $\delta B/B_{0,1} = 0.3$ , the derived distributions approximately correspond to those obtained by Heavens & Drury (1988). The presence of large amplitude perturbations ( $\delta B/B_{0,1} = 3.0$ ) has noticeable effect on the angular distributions, in comparison to the  $\delta B/B_{0,1} = 0.3$  case, only for the Kolmogorov turbulence spectrum.

#### 4. SUMMARY AND FINAL REMARKS

The present work is intended to study the first-order Fermi acceleration processes acting at relativistic shocks. To derive the stationary particle spectra we apply the test particle approach and neglect possibility of radiative losses or the second-order acceleration process acting in the turbulent medium near the shock. The hybrid method applied for a particle trajectory integration allows us to include essential characteristics of particle motion important for the acceleration process. In comparison to the previous work, we include a few ‘realistic’ features of the magnetic field turbulence. The field perturbations are imposed upon the homogenous component, which allows us to analyze conditions with different mean magnetic field inclinations to the shock normal and a range of turbulence amplitudes. We use an analytic model for the perturbations, forming the power-law spectrum within a wide wave vector range. The turbulent magnetic field is continuous across the shock — the downstream field is derived from the upstream one with the respective shock jump conditions.

The modeling shows how the resulting spectra of accelerated particles depend on the shock velocity and the turbulent magnetic field structure considered. In particular, we demonstrate effects of the finite wave vector range of the turbulence, leading to deviations of the derived spectra from the usually considered power-law form (e.g., a harder spectral component occurring at high particle energies in subluminal shocks, the spectrum steepening and the formation of the cut-off in the resonance energy range in superluminal shocks). Furthermore, we discuss the role of the long wave magnetic field perturbations in forming particle spectra. We show that the formation of locally subluminal configurations is important for a power-law spectrum generation at superluminal shocks, but long wave field perturbations lead to the significant modifications of diffusive acceleration process at parallel shocks as well. In our modeling, we reproduce also a number of previously obtained results.

In particular we demonstrate that particle spectral indices depend on the mean magnetic field configuration and on the amplitude and the wave power spectrum of field perturbations. A strong dependence of test-particle spectra on conditions at relativistic shock fronts means that reliable theoretical modeling of real astrophysical sources in which such waves occur can be difficult.

The first-order Fermi process can be applied to sufficiently energetic particles only, which have their gyroradii much larger than the dissipative thickness of the shock, defined possibly by gyroradii of thermal ions present in the plasma. Results of the present paper are valid for such high-energy particles. Particles of lower energies are expected to be accelerated by different processes, like those discussed by, e.g., Hoshino et al. (1992) or Pohl et al. (2002).

Further progress in the study of relativistic shock particle acceleration is impossible without understanding of the microphysics of relativistic shocks. A noticeable advance in this field may result from application of particle-in-cell simulations, which allow for consistent studies of the shock structure, particle injection and magnetic field generation at the shock (e.g., Drury et al. 2001; Schmitz et al. 2002; Nishikawa et al. 2003; Frederiksen et al. 2003). Realistic modeling of particle acceleration at relativistic astrophysical shocks, which have to incorporate results of such studies, requires a full plasma nonlinear description. This should take into account appropriate boundary conditions, the second-order acceleration processes, the accelerated particle influence on the shock wave structure (including possibility of the existence of the cosmic ray precursor) and the magnetic field turbulence structure in the vicinity of the shock. The Monte Carlo numerical simulations have recently been used to study nonlinear particle acceleration at shocks modified by the backreaction of accelerated particles (Ellison & Double 2002). Estimates of the effectiveness of second-order Fermi process acting in a strongly turbulent field downstream of the shock made by Dermer (2001) suggest that this process is able to produce high-energy particles. To make such models more realistic, there is a need for a detailed studies of the problem of magnetic field generation and turbulence evolution near/at the shock.

Let us also stress that the issue of MHD turbulence generation at the shock is of the great importance for ultrarelativistic shocks. Such shock waves are suggested to be the gamma-ray burst sources and may also produce ultra-high-energy cosmic rays. Modeling of the burst afterglows spectra yields often results pointing to the asymptotic spectral index  $\alpha \approx 4.3$  for radiating electrons, which is sometimes interpreted as observational confirmation of the correctness of theoretical models proposed for ultrarelativistic shock acceleration. As mentioned in Section 1, these models consider highly turbulent conditions near the shock. Standard hydrodynamical gamma-ray burst models assume the magnetic field to be generated locally at the ultrarelativistic shock (e.g., Medvedev & Loeb 1999), but the effectiveness

of the generation mechanism and the resulting perturbation spectrum is uncertain. If this effectiveness is low, the particle spectra produced at high  $\gamma$  shocks are expected to be much steeper than the asymptotic one (see Bednarz & Ostrowski 1998; and also results of our simulations for  $u_1 = 0.98c$ ). Therefore, magnetic field turbulence generation problem have to be analyzed in detail to make realistic estimates of the importance of the first-order Fermi process on the observed parameters of gamma-ray bursts. Generation of ultra-high-energy cosmic rays at such shocks requires the respective long wave field perturbations, too. It is highly uncertain if such processes take place.

We have performed our modeling in conditions defined in units of a particle gyroradius and a mean inclination of the magnetic field. The respective scaling of these conditions by choosing values for  $B_{0,1}$ ,  $\psi_1$  and the turbulence spectrum allows — at least formally — to apply these results in various astrophysical objects, as long as losses are unimportant. For situations with radiative processes playing a role, one should repeat simulations for given physical values of the model parameters and the respective radiative loss terms.

The work was supported by the Polish State Committee for Scientific Research in 2002-2004 as a research project 2 P03D 008 23 (J. N.) and in 2002-2005 as a research project PBZ-KBN-054/P03/2001 (M. O.).

### A. SHORT WAVES IN OUR HYBRID APPROACH

Short waves ( $\lambda \ll r_g$ ) influence on particle trajectories is treated here as random, small amplitude angular perturbations of particle momenta with a discrete scattering procedure described, e.g., by Ostrowski (1991). In this procedure, a particle momentum direction is perturbed at discrete instants of time by a small angle  $\Delta\Omega$ . Fitting of this approach to the magnetic field turbulence spectrum considered and varying particle energies, requires determination of the scattering probability distribution for  $\Delta\Omega$ . This is determined by additional simulations described below.

Short waves are defined as the ones with  $\lambda < \lambda_{min} = 0.05r_g(B = B_{0,1})$ . In analogy to the approach described by Ostrowski (1991), in our simulations, particle trajectory perturbations are introduced along the ‘exact’ orbit in the magnetic field composed of the mean field and turbulent fluctuations with wavelengths larger than  $\lambda_{min}$ . A particle momentum direction perturbations are performed at discrete instants of time separated by  $\Delta t$ . In the present simulations,  $\Delta t = 0.01t_g(t_g = 2\pi r_g(B = B_{0,1})/c)$ . At each scattering, the value of the scattering amplitude  $\Delta\Omega$  is selected at random from the scattering probability distribution. As  $\Delta\Omega$  stands only for the angular distance between the original and the scattered momentum

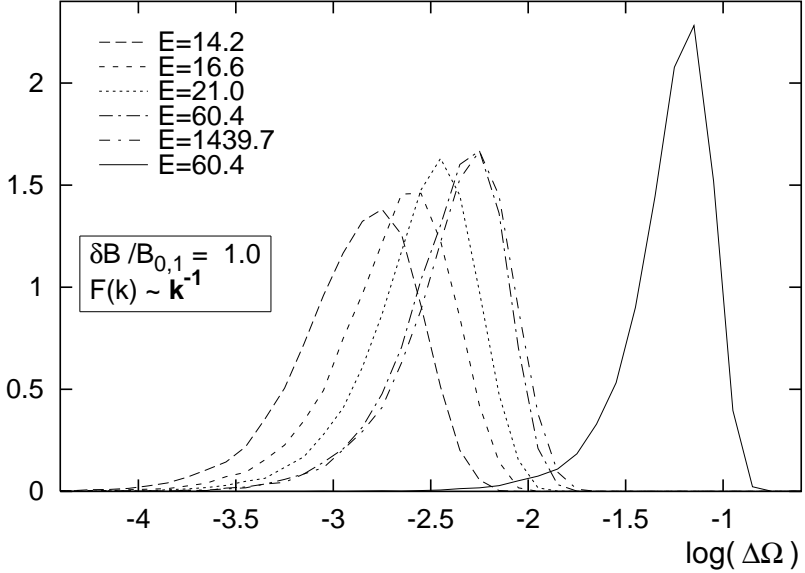


Fig. 11.— Angular scattering probability distributions for selected particle energies for the upstream turbulence amplitude  $\delta B/B_{0,1} = 1.0$  and the flat wave power spectrum. The solid line represents distribution of the full turbulent magnetic field influence on particle motion at the same time intervals. All distributions are normalized to unity.

vectors on the sphere of  $|\mathbf{p}| = const$ , one has also to specify the scattering azimuthal angle, in order to derive the scattered vector orientation. The scattering azimuthal angle is randomly chosen from the range  $[0, 2\pi]$ .

In the additional simulations determining the scattering probability distribution, a large number of particles (usually  $N = 10^4$ ) were injected at random positions and random momentum vector orientations into the turbulent magnetic field composed of the short waves only. Trajectory of each particle was subsequently integrated over the time  $\Delta t$ , when the scattering angle  $\Delta\Omega$  was derived and the particle weight ( $w = 1$ ) was added to the respective  $\log \Delta\Omega$ -bin. The scattering probability distribution obtained, was ultimately normalized to unity. Due to particle interactions with small scale field fluctuations, particle spatial positions diverge from the ‘exact’ trajectory in the magnetic field composed of the mean field and long waves. The shifts introduced are small, however, and we neglect them in order to simplify the scattering model (there are no spatial scatterings accompanying the angular ones). Since the downstream magnetic field structure is different from the upstream one the scattering probability distribution was determined independently in this region. We emphasize that the probability distribution for  $\Delta\Omega$  is not model assumed (cf. Kirk & Schneider 1987b; Ostrowski 1991), but it is determined by a particular pattern of short waves present in the simulations.

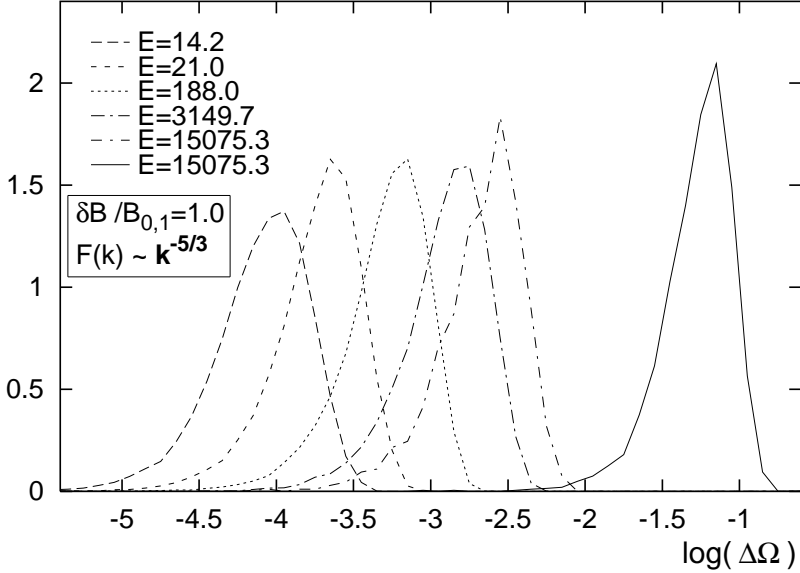


Fig. 12.— Angular scattering probability distributions for the upstream field with  $\delta B/B_{0,1} = 1.0$  and the Kolmogorov wave power spectrum. The full magnetic field influence is represented by the solid line.

In the wave vector range of the magnetic field perturbations considered, the condition for the short wave fluctuations ( $\lambda < \lambda_{min}(E)$ ) is fulfilled by different sets of waves for different particle energies. The scattering conditions and, consequently, the scattering probability distribution vary continuously with a particle energy. In our simulations, we calculate these probability distributions for a discrete set of energies. As our turbulent field is modeled by a discrete wave power spectrum, the consecutive energies are selected in such a way that corresponding short wave turbulent fields differ by a few waves only. In effect, each subsequent distribution differs modestly from the previous one. Example scattering probability distributions are presented in Figure 11 for the upstream field with  $\delta B/B_{0,1} = 1.0$  and the flat wave power spectrum. The mean scattering angle due to short wave perturbations increases with a particle energy, but it is small in comparison with the full (including all waves) magnetic field influence on particle motion, represented in the figure by the full line for the selected  $E = 60.4$ .

In Figure 11, the probability distributions corresponding to highest energies overlap, which indicates similar scattering conditions at these energies. In fact, the most efficient scattering is provided by the long-wavelength part of the short waves considered at any given particle energy, whereas smallest scales do not contribute significantly to a trajectory perturbations. In the turbulent magnetic field with the flat wave power spectrum, the field energy in the waves responsible for scattering is similar for higher-energy particles, which

results in statistically identical scattering probability distributions in a wide energy range. This is not the case for the Kolmogorov wave spectrum, where the scattering conditions vary with a particle energy, leading to the variations of the scattering probability distribution, as shown in Figure 12. As one can see, the mean perturbation angle increases continuously with a particle energy in this case. Finally, for the highest particle energies, all the waves form the small scale turbulence and the mean perturbation angle starts to decrease.

## B. TESTS OF THE SIMULATION METHOD

The Runge-Kutta routine we use for trajectory integration is accurate to fifth order. The embedded fourth-order formula estimates the truncation error at a given point of a particle orbit, what allows for an appropriate stepsize adjustment, to ensure integration with the accuracy required. We have set the truncation error at every integration step to be less than  $10^{-7}$ . The accuracy imposed allows for a precise and an efficient trajectory calculation. With this choice, a particle energy between shock crossings is conserved to better than one part in  $10^7$ . Integration with small, but still finite accuracy, produces inevitably the numerical noise, which influences stability of calculated trajectories. This noise can be regarded as resulted from an additional small scale magnetic field turbulence. We have checked, via diffusion coefficients derivations (see Ostrowski 1993), that the energy density in these fluctuations is small and do not change noticeably the wave power spectrum assumed for the simulations. Our trajectories are stable over at least several particle gyroperiods. In the vicinity of a relativistic shock wave, very few particles which form the spectrum stay on either side of the shock front for many gyroperiods between successive shock crossings. The exception may be particles of energy near the injection energy  $E_0$ , which only weakly interact with the turbulent field. However, the part of the spectrum formed by these particles is already influenced by the initial conditions.

In order to check if the method of particle spectra and angular distributions measurement works properly, additional simulations were performed. An isotropic particle source was located at some point in the plasma. On both sides of that point a set of 5 parallel barriers was placed, every one several particle gyroradii away from each other. Trajectories of  $N = 1000$  particles originated at the particle source were subsequently calculated then. Every time a particle crossed one of the barriers, a quantity  $1/(|v_x| + 0.005)$  was added to the respective  $\cos(\theta)$ -bins, where  $\theta$  is the angle between the particle momentum and the normal to a given barrier. Trajectory calculations were finished when a particle escaped far from the external barriers. The resulted particle angular distribution, averaged over 10 different sets of particles and realizations of the turbulent magnetic field, was isotropic, as expected.

Small departures from isotropy due to statistical errors occurred only near  $\cos \theta \approx 0$ , so that angular distributions presented in Section 3 might be measured with worse quality near that value of  $\cos \theta$ . These simulations were performed for the upstream turbulent magnetic field with  $\delta B/B_{0,1} = 1.0$  and the flat wave power spectrum.

In our hybrid approach, used for a particle trajectory integration, the short waves, both upstream and downstream of the shock, are defined by a particle gyroradius in the *upstream* mean magnetic field ( $\lambda < \lambda_{min} = 0.05 r_g(B = B_{0,1})$ ). However, in cases of higher turbulence amplitudes, the average magnetic field can be much higher than  $B_{0,1}$ , especially downstream of the shock, where the magnetic field is amplified by compression. Particle gyroradii are then respectively smaller than  $r_g(B = B_{0,1})$ . In effect, some part of the resonance wave vectors for a particle of a given energy is treated in the simulations as a short wave turbulence, whose influence on particle trajectories is modeled by the scattering terms. In order to check if the definition of short waves used in our simulations does not generate false results, additional simulations were done with the modified definitions of short wave perturbations. We have checked all the spectra presented in the paper for the upstream turbulence amplitude  $\delta B/B_{0,1} = 3.0$ . For this perturbation amplitude, the average upstream magnetic field is equal to  $\langle B_1 \rangle \approx 2.3$  and the definition of short waves we adopted is  $\lambda < \lambda_{min} = 0.02 r_g(B = B_{0,1})$  in this case. The average magnetic field value downstream of the shock depends on the mean field configuration and the compression factor  $r$ . For parallel shocks propagating with velocity  $u_1 = 0.5c$ ,  $\langle B_2 \rangle \approx 10$  and the definition of short waves is  $\lambda < \lambda_{min} = 0.005 r_g(B = B_{0,1})$ . For the above definitions of the short wave turbulence, the scattering probability distributions have been determined. The particle spectra obtained in the test simulations with the modified definition of short waves are, in the limit of statistical accuracy, the same as those calculated in the simulations with unmodified definition of small scale perturbations<sup>6</sup>.

The most important test concerns the hybrid approach we use in the simulations. A straightforward way to check if it gives the correct results would be to perform simulations by integrating exact particle trajectories in the magnetic field with all the turbulence scales present, without introducing the scattering terms. However, it was impossible to perform such modeling with the full range of wave vectors considered ( $k_{max}/k_{min} = 10^5$ ) because of the excessive simulation time required. In this situation, we have performed such simulations for a limited wave vector range, with  $k_{min} = 0.01$  and  $k_{max} = 10$ . We have investigated the acceleration process at the shock wave moving with velocity  $u_1 = 0.5c$ , the mean upstream

---

<sup>6</sup>The value of the average downstream magnetic field can be larger for faster shocks (e.g. for  $u_1 = 0.9c$ ,  $\psi_1 = 45^\circ$ ,  $\langle B_2 \rangle \approx 16$ ), so the required  $\lambda_{min}$  should be respectively smaller. However, for such small  $\lambda_{min}$  the simulation time would be very long.

magnetic field inclined at the angle  $\psi_1 = 45^\circ$  to the shock normal and the amplitude of the field turbulence  $\delta B/B_{0,1} = 1.0$  with the flat wave power spectrum. In addition, parallel simulations were performed with the use of the original hybrid approach, with the same simulation parameters. Both methods yielded the same results within the statistical accuracy: the particle spectrum is a power-law in a finite energy range, followed by the harder component. Statistical accuracy of the spectral index calculation for the modeling without scattering terms was here rather low, because these simulations have been performed for only one set of  $N = 100$  injected particles and one realization of the turbulent magnetic field.

## REFERENCES

Achterberg, A., Gallant, Y. A., Kirk, J. G., & Guthmann, A. W. 2001, MNRAS, 328, 393

Ballard, K. R., & Heavens, A. 1992, MNRAS, 259, 89

Bednarz, J., & Ostrowski, M. 1996, MNRAS, 283, 447

Bednarz, J., & Ostrowski, M. 1998, Phys. Rev. Lett., 80, 3911

Begelman, M. C., & Kirk, J. G. 1990, ApJ, 353, 66

Cho, J. 2001, J. Korean Astron. Soc., 34, S275

Cho, J., Lazarian, A., & Vishniac, E. T. 2003, ApJ, 595, 812

Decker, R. B., & Vlahos, L. 1985, J. Geophys. Res., 90, 47

Dermer, C. D. 2001, in Proc. 27th Int. Cosmic Ray Conf., ed. K.-H. Kampert, G. Heinzelmann, & C. Spiering (Hamburg: Copernicus Gessellschaft), 2039

Drury, L. O’C. 1983, Rep. Prog. Phys., 46, 973

Drury, L. O’C., McClements, K. G., Chapman, S. C., Dendy, R. O., Dieckmann, M. E., Lyung, P., & Ynnerman, A. 2001, in Proc. 27th Int. Cosmic Ray Conf., ed. K.-H. Kampert, G. Heinzelmann, & C. Spiering (Hamburg: Copernicus Gessellschaft), 2096

Ellison, D. C., Jones, F. C., & Reynolds, S. P. 1990, ApJ, 360, 702

Ellison, D. C., & Double, G. P. 2002, Astroparticle Phys., 18, 213

Frederiksen, J. T., Hededal, C., Haugbolle, T., & Nordlund, A. 2003, preprint (astro-ph/0303360)

Gallant, Y. A., & Achterberg, A. 1999, MNRAS, 305, L6

Gallant, Y. A., Achterberg, A., & Kirk, J. G. 1999, A&AS, 138, 549

Giacalone, J., & Jokipii, J. R. 1994, ApJ, 430, L137

Heavens, A., & Drury, L. O’C. 1988, MNRAS, 235, 997

Hoshino, M., Arons, J., Gallant, Y. A., & Langdon, A. B. 1992, ApJ, 390, 454

Kirk, J. G., Guthmann, A. W., Gallant, Y. A., & Achterberg, A. 2000, ApJ, 542, 235

Kirk, J. G., & Heavens, A. 1989, MNRAS, 239, 995

Kirk, J. G., & Schneider, P. 1987a, ApJ, 315, 425

Kirk, J. G., & Schneider, P. 1987b, ApJ, 322, 256

Lagage, P. O., & Cesarsky, C. J. 1983, A&A, 118, 223

Leamon, R. J., Smith, C. W., Ness, N. F., Matthaeus, W. H., & Wong, H. K. 1998, J. Geophys. Res., 103, 4775

Lee, L. C., & Jokipii, J. R. 1976, ApJ, 206, 735

Lemoine, M., & Pelletier, G. 2003, ApJ, 589, L73

Lucek, S. G., & Bell, A. R. 2000, MNRAS, 314, 65

Medvedev, M. V., & Loeb, A. 1999, ApJ, 526, 697

Naito, T., & Takahara, F. 1995, MNRAS, 275, 1077

Nishikawa, K.-I., Hardee, P., Richardson, G., Preece, R., Sol, H., & Fishman, G. J. 2003, ApJ, 595, 555

Ostrowski, M. 1988a, MNRAS, 233, 257

Ostrowski, M. 1988b, A&A, 206, 169

Ostrowski, M. 1991, MNRAS, 249, 551

Ostrowski, M. 1993, MNRAS, 264, 248

Ostrowski, M. 2002, J. Phys. Studies, 6, 393 (astro-ph/0310833)

Ostrowski, M., & Bednarz, J. 2002, A&A, 394, 1141

Pohl, M., Lerche, R., & Schlickeiser, R. 2002, A&A, 383, 829

Press, W., Teukolsky, S. A., Vetterling, W. T., & Flannery B. P. 1992, Numerical Recipes in FORTRAN 77 (2d ed.; Cambridge: Cambridge University Press)

Schmitz, H., Chapman, S. C., & Dendy, R. O. 2002, ApJ, 570, 637

Stinebring, D. R., Smirnova, T. V., Hankins, T. H., Hovis, J. S., Kaspi, V. M., Kempner, J. C., Myers, E., & Nice, D. J. 2000, ApJ, 539, 300

Webb, G. M., Axford, W. I., & Terasawa, T. 1983, ApJ, 270, 537

Table 1. Spectral indices obtained for parallel shocks with  $u_1 = 0.5c$

$\delta B/B_{0,1}$	Spectral Index $\alpha$	
	$q = 0$	$q = 5/3$
$\ll 1$ (analytic) <sup>a</sup>	3.72	3.74
0.3	3.65	3.61
1.0	3.45	3.47
3.0	3.59	3.62

<sup>a</sup>Values of  $\alpha$  calculated by Heavens & Drury (1988) for small amplitude perturbations,  $\delta B/B_{0,1} \ll 1$ .